

A Diagnostic Framework for Implementation Risk in Bilevel Decision Problems: The Ambiguity Premium and the Robustness–Efficiency Frontier

Jiguang Yu
jyu678@bu.edu¹

¹College of Engineering, Boston University, Boston, MA 02215, USA

May 19, 2026

Abstract

Hierarchical decision problems are often modeled as bilevel programs in which a leader commits to a policy and a follower responds optimally. When the follower’s optimal response is nonunique, or when only near-optimal follower behavior can be verified, the same leader decision may induce a range of upper-level outcomes. This paper develops a diagnostic framework for quantifying that exposure. For a leader decision x , we evaluate the optimistic and pessimistic upper-level values over the ϵ -optimal follower response set $S_\epsilon(x)$ and use their difference,

$$\Delta_\epsilon(x) := \psi_\epsilon^p(x) - \psi_\epsilon^o(x),$$

as an ambiguity premium. The premium itself is classical in the optimistic–pessimistic bilevel distinction; the contribution here is to make it operational as an implementation-risk diagnostic. We establish a diameter bound $\Delta_\epsilon(x) \leq L_F(x) \text{diam}(S_\epsilon(x))$ and an $O(\sqrt{\epsilon})$ estimate under quadratic lower-level growth. We then organize existing bilevel–GNEP reformulations by their computational roles and propose a screening workflow that reports, for each candidate policy, nominal value, ambiguity exposure, and a first-order residual. Two stylized case studies—a parallel-link Stackelberg pricing problem and a convex generation-planning model with diversification constraints—show how the resulting robustness–efficiency frontier can identify policies that are nominally attractive but sensitive to near-optimal follower responses.

Keywords: bilevel optimization; Stackelberg games; generalized Nash equilibrium; optimistic and pessimistic bilevel; implementation risk; parametric stability; robustness–efficiency frontier.

1 Introduction

Bilevel optimization is a natural modeling framework for hierarchical decision problems in which one agent commits to a policy and a second agent reacts optimally [1–8]. Such structures arise in Stackelberg games and network pricing [9–12], regulation [13, 14], infrastructure planning and energy systems [15–18], interdiction and security [19–22], hyperparameter and machine-learning pipelines [23–25], and many other areas. Their appeal is also their main difficulty: the leader’s feasible region is defined implicitly through the follower’s solution map, and the upper-level outcome may depend critically on how lower-level optimal responses are selected. This is especially acute when the follower admits multiple optima, giving rise to the classical distinction between optimistic and pessimistic bilevel models [5, 26–35].

Motivation. From a decision-maker’s perspective, follower nonuniqueness is not merely a technical nuisance. Two follower responses that are equally acceptable from the follower’s point of view can induce materially different upper-level outcomes. Moreover, in many real systems the leader can only verify that a follower’s response is approximately optimal: numerical tolerances, bounded rationality, contractual flexibility, or simply the existence of multiple equally good operating points all create a neighborhood of acceptable follower responses rather than a single point. Denoting this ϵ -optimal response set by $S_\epsilon(x)$, the relevant quantity for a planner is not only the nominal leader value, but also the width of the leader’s *value interval* $[\psi_\epsilon^o(x), \psi_\epsilon^p(x)]$ generated by $S_\epsilon(x)$.

Contribution. The optimistic–pessimistic value gap is a classical object in bilevel optimization. Our contribution is not to introduce this gap, but to use it as the organizing quantity in a decision diagnostic for implementation risk. Specifically, we make four contributions.

First, we define a candidate-level diagnostic triple consisting of nominal optimistic value, ambiguity exposure, and a first-order residual, and we summarize the first two components through a robustness–efficiency frontier. Second, we connect the ambiguity premium to response-set geometry by proving a Lipschitz diameter bound and an $O(\sqrt{\epsilon})$ estimate under quadratic lower-level growth. Third, we organize existing bilevel–GNEP reformulations [36–39] according to their computational roles: global optimistic reformulation, stationarity-oriented computation, and pessimistic lower-equilibrium evaluation. Fourth, we demonstrate the workflow on two stylized examples chosen to isolate different sources of ambiguity: exact follower multiplicity in a Stackelberg pricing problem and near-optimal redispatch in a strictly convex planning problem.

The analytical role of the paper is to collect simple stability consequences of the diagnostic and make them operational for screening candidate leader decisions. The computational workflow uses Nikaido–Isoda-type penalization [40, 41] for pessimistic evaluation and a proximal alternating scheme for optimistic candidate generation, with a Fischer–Burmeister residual [42, 43] replacing ad hoc residuals.

Scope. The framework is diagnostic rather than predictive. We do not claim new bilevel–GNEP equivalence theorems, nor do we claim global optimality for all numerically reported pessimistic portfolios. The reformulations used below are drawn from the existing GNEP and bilevel literature. The case studies are stylized computational experiments designed to show how the diagnostic behaves, not empirical forecasts or policy recommendations.

Positioning relative to recent literature. Recent work has greatly expanded the scope of bilevel analysis under uncertainty and equilibrium [30, 32, 44, 45], has produced improved global solution methods for optimistic and pessimistic problems [46–50], and has clarified the role of generalized Nash equilibria in hierarchical settings [51–53]. Our framework is complementary to this computational work: it takes the existence of such solvers as a given and adds a decision-analytic overlay that evaluates a candidate decision along three dimensions at once.

Organization. Section 2 fixes notation, consolidates definitions of the lower-level value function and solution map, and defines the decision diagnostics. Section 3 presents the analytical results linking the ambiguity premium to diameter and quadratic-growth moduli. Section 4 reviews the three GNEP reformulations used in the workflow and states their computational roles. Section 5 describes the computational workflow. Sections 6–7 present the two case studies. Section 8 discusses managerial implications with softened claims. Section 9 concludes. Appendix A contains proofs; Appendix B documents reproducibility.

2 Problem Class, Value Functions, and Diagnostics

We consider a parametric bilevel setting with leader decision $x \in X \subset \mathbb{R}^n$ and follower decision $y \in Y \subset \mathbb{R}^m$. We make the following standing assumption throughout the paper, which is mild and standard [6, 54].

Assumption 2.1 (Standing assumptions). $X \subset \mathbb{R}^n$ and $Y \subset \mathbb{R}^m$ are nonempty compact sets. $F : X \times Y \rightarrow \mathbb{R}$ and $f : X \times Y \rightarrow \mathbb{R}$ are continuous.

Under Assumption 2.1, the lower-level value function and exact solution map

$$\phi(x) := \min_{v \in Y} f(x, v), \quad S(x) := \arg \min_{v \in Y} f(x, v) = \{y \in Y : f(x, y) = \phi(x)\} \quad (1)$$

are well defined, ϕ is continuous on X , and S is nonempty-valued and upper semicontinuous [54]. The ϵ -optimal response set for $\epsilon \geq 0$ is

$$S_\epsilon(x) := \{y \in Y : f(x, y) \leq \phi(x) + \epsilon\}. \quad (2)$$

By construction $S(x) = S_0(x) \subseteq S_{\epsilon_1}(x) \subseteq S_{\epsilon_2}(x) \subseteq Y$ for $0 \leq \epsilon_1 \leq \epsilon_2$.

The optimistic and pessimistic leader value functions at tolerance $\epsilon \geq 0$ are

$$\psi_\epsilon^o(x) := \min_{y \in S_\epsilon(x)} F(x, y), \quad (3)$$

$$\psi_\epsilon^p(x) := \max_{y \in S_\epsilon(x)} F(x, y). \quad (4)$$

Both the minimum and the maximum are attained under Assumption 2.1, because $S_\epsilon(x)$ is a nonempty compact subset of Y and $F(x, \cdot)$ is continuous. The ambiguity premium is

$$\Delta_\epsilon(x) := \psi_\epsilon^p(x) - \psi_\epsilon^o(x) \geq 0. \quad (5)$$

2.1 Decision diagnostics

We assemble the quantities used to compare candidate leader decisions into the following decision-diagnostic set.

Definition 2.2 (Decision diagnostics). For $x \in X$, $y \in Y$, and $\epsilon \geq 0$:

1. *Ambiguity premium*: $\Delta_\epsilon(x) = \psi_\epsilon^p(x) - \psi_\epsilon^o(x)$.
2. *Normalized ambiguity ratio*: $\rho_\epsilon(x) := \Delta_\epsilon(x)/(1 + |\psi_\epsilon^o(x)|)$.
3. *Tolerance violation residual*:

$$r_{LL}^\epsilon(x, y) := \max\{0, f(x, y) - \phi(x) - \epsilon\}. \quad (6)$$

4. *Stationarity residual*. The definition of a usable first-order residual requires some care because ϕ is continuous but generally nondifferentiable. We therefore define the stationarity residual through the GNEP reformulation (G1) of Section 4, which avoids $\nabla_x \phi$. Concretely, at a triple $(x, y, v) \in X \times Y \times Y$ with multiplier $\lambda \geq 0$ on the coupling constraint $h(x, y, v) := f(x, y) - f(x, v) - \epsilon \leq 0$, we use only first derivatives of f and F , which are well defined whenever F and f are continuously differentiable on a neighborhood of the candidate point.

Remark 2.3 (Assumptions where they are used). The standing assumptions (compactness and continuity) are used for Definition 2.2(a)–(c). Definition 2.2(d) is well defined only under the additional smoothness assumption that F and f are continuously differentiable in (x, y) on a neighborhood of the candidate point; we make this assumption explicit when the stationarity residual is used, and not globally.

We also use the Pareto set in the plane $(\psi_\epsilon^o, \Delta_\epsilon)$:

$$\mathcal{P}_\epsilon := \{(\psi_\epsilon^o(x), \Delta_\epsilon(x)) : x \in X, x \text{ is not dominated}\}, \quad (7)$$

where (u, δ) dominates (u', δ') iff $u \leq u'$, $\delta \leq \delta'$, and at least one inequality is strict. We call \mathcal{P}_ϵ the robustness–efficiency frontier. Its practical utility is that it compresses the joint evaluation of nominal value and implementation exposure into a two-dimensional picture without throwing away either dimension.

3 Structural Properties of the Ambiguity Premium

This section contains the main analytical contribution of the paper. The results are not deep, but they link the ambiguity premium to standard stability quantities and therefore give the diagnostic analytical content beyond its definitional form.

Throughout, let $\text{diam}(A) := \sup_{y, y' \in A} \|y - y'\|$ denote the diameter of a nonempty bounded set $A \subseteq \mathbb{R}^m$.

3.1 Attainment and interval width

Proposition 3.1 (Attainment and interval width). *Under Assumption 2.1, for every $x \in X$ and $\epsilon \geq 0$ the set $S_\epsilon(x)$ is nonempty and compact; both $\psi_\epsilon^o(x)$ and $\psi_\epsilon^p(x)$ are attained; and*

$$\Delta_\epsilon(x) = \text{diam}_{\mathbb{R}}(F(x, S_\epsilon(x))) = \max_{y \in S_\epsilon(x)} F(x, y) - \min_{y \in S_\epsilon(x)} F(x, y), \quad (8)$$

where $\text{diam}_{\mathbb{R}}(A) := \sup A - \inf A$ is the one-dimensional diameter of a bounded nonempty $A \subseteq \mathbb{R}$.

Proof. Nonemptiness of $S(x) \subseteq S_\epsilon(x)$ and compactness follow from continuity of $f(x, \cdot)$ on the compact set Y . The image $F(x, S_\epsilon(x))$ is then a nonempty compact subset of \mathbb{R} , so its supremum and infimum are attained and $\Delta_\epsilon(x) = \sup F(x, S_\epsilon(x)) - \inf F(x, S_\epsilon(x))$. \square

3.2 Monotonicity in follower tolerance

Proposition 3.2 (Monotonicity). *Fix $x \in X$. For $0 \leq \epsilon_1 \leq \epsilon_2$: $S_{\epsilon_1}(x) \subseteq S_{\epsilon_2}(x)$, $\psi_{\epsilon_2}^o(x) \leq \psi_{\epsilon_1}^o(x)$, $\psi_{\epsilon_2}^p(x) \geq \psi_{\epsilon_1}^p(x)$, and $\Delta_{\epsilon_2}(x) \geq \Delta_{\epsilon_1}(x)$.*

Proof. If $y \in S_{\epsilon_1}(x)$, then $f(x, y) \leq \phi(x) + \epsilon_1 \leq \phi(x) + \epsilon_2$, so $y \in S_{\epsilon_2}(x)$. By Proposition 3.1 the minima and maxima are attained, so minimization over a larger set cannot increase the minimum and maximization cannot decrease the maximum. The stated inequalities follow. \square

3.3 A diameter-based Lipschitz bound

The following bound is elementary but useful as a diagnostic device: it connects the ambiguity premium to a response-set geometry quantity (the diameter of the ϵ -response set) and a leader-side Lipschitz modulus. We present it as a diagnostic bound rather than a deep structural theorem.

Theorem 3.3 (Diameter-based bound). *Assume $F(x, \cdot)$ is $L_F(x)$ -Lipschitz continuous on Y , i.e.*

$$|F(x, y) - F(x, y')| \leq L_F(x) \|y - y'\| \quad \forall y, y' \in Y. \quad (9)$$

Then for every $\epsilon \geq 0$

$$\Delta_\epsilon(x) \leq L_F(x) \cdot \text{diam}(S_\epsilon(x)). \quad (10)$$

Proof. By Proposition 3.1 there exist $y^+, y^- \in S_\epsilon(x)$ with $F(x, y^+) = \psi_\epsilon^p(x)$ and $F(x, y^-) = \psi_\epsilon^o(x)$. Then

$$\Delta_\epsilon(x) = F(x, y^+) - F(x, y^-) \leq L_F(x) \|y^+ - y^-\| \leq L_F(x) \text{diam}(S_\epsilon(x)).$$

□

Theorem 3.3 has two useful consequences. First, one can upper-bound implementation risk with any tractable bound on the diameter of the ϵ -response set, regardless of the specific leader objective. Second, the modulus $L_F(x)$ is explicitly computable in most applications (e.g., $L_F(x)$ can be taken as a bound on $\|\nabla_y F(x, \cdot)\|$ on Y).

3.4 Rate under quadratic growth

The diameter bound is most informative when $S_\epsilon(x)$ shrinks with ϵ . A standard sufficient condition for this is quadratic growth of the lower-level objective around its optimal set [54–56].

Assumption 3.4 (Quadratic lower-level growth). There exists $\mu(x) > 0$ such that

$$f(x, y) \geq \phi(x) + \mu(x) \text{dist}(y, S(x))^2 \quad \forall y \in Y. \quad (11)$$

If Y is convex and $f(x, \cdot)$ is $2\mu(x)$ -strongly convex on Y , then $S(x)$ is a singleton and Assumption 3.4 holds with the displayed $\mu(x)$. More generally, quadratic growth is a standard ingredient of error-bound theory [55–57] and holds under a variety of second-order sufficient conditions that do not require convexity of the lower-level objective.

Corollary 3.5 ($O(\sqrt{\epsilon})$ rate). Under Assumptions 2.1, (9), and 3.4,

$$\text{diam}(S_\epsilon(x)) \leq \text{diam}(S(x)) + 2\sqrt{\epsilon/\mu(x)}, \quad (12)$$

and

$$\Delta_\epsilon(x) \leq L_F(x) \left(\text{diam}(S(x)) + 2\sqrt{\epsilon/\mu(x)} \right). \quad (13)$$

If in addition $S(x) = \{y^*(x)\}$ is a singleton, then $\Delta_\epsilon(x) \leq 2L_F(x)\sqrt{\epsilon/\mu(x)}$.

Proof. For any $y \in S_\epsilon(x)$, quadratic growth gives $\mu(x) \text{dist}(y, S(x))^2 \leq f(x, y) - \phi(x) \leq \epsilon$, so $\text{dist}(y, S(x)) \leq \sqrt{\epsilon/\mu(x)}$. Hence $S_\epsilon(x) \subseteq S(x) + B(0, \sqrt{\epsilon/\mu(x)})$. The diameter bound $\text{diam}(S_\epsilon(x)) \leq \text{diam}(S(x)) + 2\sqrt{\epsilon/\mu(x)}$ follows from the triangle inequality. Combining with (10) yields (13). The singleton case gives $\text{diam}(S(x)) = 0$. □

Remark 3.6 (Local versus global quadratic growth). Assumption 3.4 is stated globally on Y . For the $O(\sqrt{\epsilon})$ rate as $\epsilon \downarrow 0$, only a local form is needed: it suffices that the inequality (11) holds on a neighborhood of $S(x)$ in Y , with the constant $\mu(x)$ adapted to that neighborhood. The global form is mathematically safer but strictly stronger than what is required.

Remark 3.7 (Interpretation). Corollary 3.5 explains why the ambiguity premium in the strictly convex case study of Section 7 scales roughly like $\sqrt{\epsilon}$ and remains positive even when the exact follower optimum is unique. It also identifies the two modeling levers a designer has for controlling implementation risk: reducing $L_F(x)$ (flatten the leader objective along likely redispach directions) or increasing $\mu(x)$ (sharpen the lower-level objective).

3.5 Semicontinuity and continuity under response-set continuity

The following semicontinuity result is used below to justify the use of sampling-based frontier approximations. Note that the optimistic and pessimistic value functions have opposite semicontinuity directions in general; full continuity of both requires continuity of the correspondence $(x, \epsilon) \mapsto S_\epsilon(x)$ in the sense required by Berge's maximum theorem.

Proposition 3.8 (Semicontinuity and continuity under response-set continuity). *Under Assumption 2.1, the correspondence*

$$(x, \epsilon) \mapsto S_\epsilon(x) := \{y \in Y : f(x, y) \leq \phi(x) + \epsilon\}$$

has nonempty compact values and is upper semicontinuous on $X \times [0, \infty)$. Furthermore, the marginal functions ψ_ϵ^p and Δ_ϵ are upper semicontinuous, and ψ_ϵ^o is lower semicontinuous, in (x, ϵ) .

If, in addition, Assumption 3.4 holds and there exists a neighborhood U of x_0 and a constant $\underline{\mu} > 0$ such that

$$\mu(x) \geq \underline{\mu} \quad \text{for all } x \in U \cap X,$$

then $S_\epsilon(x)$ is lower semicontinuous at $(x_0, 0)$.

Moreover, if we additionally assume that Y is convex and $f(x, \cdot)$ is convex on Y for all x near x_0 , then $S_\epsilon(x)$ is lower semicontinuous at (x_0, ϵ_0) for any $\epsilon_0 > 0$.

Consequently, under these combined conditions, ψ_ϵ^o , ψ_ϵ^p , and Δ_ϵ are continuous at (x_0, ϵ_0) for all $\epsilon_0 \geq 0$.

3.6 A formal local expansion under stronger regularity

The bound in Corollary 3.5 is order-of-magnitude. Under stronger regularity one can describe the leading-order behavior of $\Delta_\epsilon(x)$ in ϵ more precisely. We present the discussion as a formal local expansion in the spirit of classical second-order sensitivity analysis [54, 58, 59] rather than as a general theorem; the relevant structural conditions can fail at active constraints or under degeneracy.

Throughout this subsection we assume the singleton case $S(x) = \{y^*(x)\}$, f twice continuously differentiable on a neighborhood of $y^*(x)$ in Y , and a second-order sufficient condition at $y^*(x)$. Let $\mathcal{T}_Y(y^*(x))$ denote the tangent cone to Y at $y^*(x)$. Following standard practice [54], define the critical cone of zero first-order increase

$$\mathcal{C}(x) := \{d \in \mathcal{T}_Y(y^*(x)) : \nabla_y f(x, y^*(x))^\top d = 0\}. \quad (14)$$

Under standard constraint qualifications and local uniqueness, the dominant $\sqrt{\epsilon}$ part of the sublevel-set displacement at $y^*(x)$ is governed by the trust-region-type set

$$D(x) := \{d \in \mathcal{C}(x) : \frac{1}{2} d^\top \nabla_{yy}^2 f(x, y^*(x)) d \leq 1\}. \quad (15)$$

Along noncritical feasible directions, f has nonzero first-order growth, so the sublevel displacement is at most $O(\epsilon)$ rather than $O(\sqrt{\epsilon})$; the $\sqrt{\epsilon}$ contribution therefore comes from $\mathcal{C}(x)$.

Formally, when the first-order variation of F along the critical cone is nonzero, the leading contribution to $\Delta_\epsilon(x)$ takes the form

$$\Delta_\epsilon(x) = \sqrt{\epsilon} \left[\sup_{d \in D(x)} \nabla_y F(x, y^*(x))^\top d - \inf_{d \in D(x)} \nabla_y F(x, y^*(x))^\top d \right] + o(\sqrt{\epsilon}). \quad (16)$$

This expression involves two trust-region-type subproblems and is computable from local first- and second-order data of F and f at $y^*(x)$. When $D(x)$ is centrally symmetric—for instance, when no inequality constraint of the lower-level problem is active at $y^*(x)$, so that $\mathcal{C}(x)$ is a linear subspace and $D(x)$ is an ellipsoid—(16) reduces to

$$\Delta_\epsilon(x) = 2\sqrt{\epsilon} \sup_{d \in D(x)} \nabla_y F(x, y^*(x))^\top d + o(\sqrt{\epsilon}). \quad (17)$$

In the presence of active inequality constraints, $\mathcal{C}(x)$ need not be a subspace and $D(x)$ need not be symmetric, in which case the general form (16) is required. We do not use (16)–(17) elsewhere in the paper; they are recorded here to indicate that the order-of-magnitude bound of Corollary 3.5 can in principle be sharpened.

4 Equilibrium Reformulations: Background and Roles

The preceding section treats $\Delta_\epsilon(x)$ as a mathematical object attached to a fixed leader decision. To use it as a practical screening diagnostic, one must compute or approximate $\psi_\epsilon^o(x)$ and $\psi_\epsilon^p(x)$ repeatedly across candidate decisions. This section recalls three existing bilevel–GNEP reformulations and assigns each a computational role in that task. The purpose is not to establish new equivalence results, but to make explicit which reformulation supports which part of the diagnostic workflow.

The results used here are taken from [37–39]; see also [36, 52, 53, 60, 61] for the GNEP machinery.

Recall the coupling constraint $g_\epsilon(x, y) = f(x, y) - \phi(x) - \epsilon$.

Standing smoothness assumptions for this section. For all KKT displays in this section, assume in addition that X and Y are closed convex sets and that F and f are continuously differentiable on a neighborhood of every candidate point. If X or Y is nonconvex, the same formal expressions should be interpreted with an appropriate limiting normal cone (Mordukhovich or Clarke) and the corresponding constraint qualifications; we do not develop the nonconvex case further.

4.1 Optimistic model: global-solution reformulation (G1)

The two-player GNEP

$$\begin{aligned} \text{Player 1: } & \min_{x, y} F(x, y) \quad \text{s.t. } x \in X, y \in Y, f(x, y) \leq f(x, v) + \epsilon, \\ \text{Player 2: } & \min_v f(x, v) \quad \text{s.t. } v \in Y, \end{aligned} \quad (\text{G1})$$

has the property that, at any equilibrium (x^*, y^*, v^*) , player 2’s optimality gives $f(x^*, v^*) = \phi(x^*)$ and hence $f(x^*, y^*) \leq \phi(x^*) + \epsilon$, so (x^*, y^*) is feasible for the optimistic bilevel problem. The equivalence between (G1) and the optimistic bilevel problem is not, however, a formal consequence of the displayed constraints alone. Under player-1 deviations the constraint $f(x, y) \leq f(x, v) + \epsilon$ is evaluated at fixed v , so it does not by itself encode $f(x, v) = \phi(x)$. Equivalence with global optimistic solutions relies on the structural assumptions stated in [37], which ensure that equilibria of the game select globally valid optimistic bilevel solutions. We use (G1) only as a conceptual device for defining a stationarity residual and for organizing the computational workflow; all equivalence claims are inherited from the cited results.

KKT system. Let $\lambda \geq 0$ be player 1's multiplier on the coupling constraint $h(x, y, v) := f(x, y) - f(x, v) - \epsilon \leq 0$, and note that player 1 controls (x, y) while player 2 controls v . No coupling multiplier appears in player 2's problem, because player 2's feasible set Y does not depend on (x, y) . The KKT system of the GNEP is

$$0 \in \nabla_x F(x, y) + \lambda(\nabla_x f(x, y) - \nabla_x f(x, v)) + N_X(x), \quad (18)$$

$$0 \in \nabla_y F(x, y) + \lambda \nabla_y f(x, y) + N_Y(y), \quad (19)$$

$$0 \in \nabla_v f(x, v) + N_Y(v), \quad (20)$$

$$0 \leq \lambda \perp f(x, y) - f(x, v) - \epsilon \leq 0. \quad (21)$$

We need to emphasize that in (20) player 2 minimizes $f(x, \cdot)$ on Y and sees no coupling constraint; this is the source of the identity $f(x^*, v^*) = \phi(x^*)$ at equilibrium.

4.2 Optimistic model: convexified stationarity reformulation (G2)

Replacing $f(x, v)$ in the coupling constraint by its first-order lower approximation in the x -variable yields

$$\text{Player 1: } \min_{x, y} F(x, y) \quad \text{s.t. } x \in X, y \in Y, f(x, y) \leq f(u, v) + \nabla_1 f(u, v)^\top (x - u) + \epsilon, \quad (G2)$$

$$\text{Player 2: } \min_{u, v} f(x, v) \quad \text{s.t. } u = x, v \in Y.$$

Under the structural assumptions stated in [38]—which include convexity of $f(\cdot, y)$ in the leader variable and appropriate constraint qualifications—solutions of (G2) correspond to stationary points of the optimistic bilevel problem and vice versa. We do not reproduce these conditions here, and we use (G2) computationally as a stationarity-targeting heuristic.

4.3 Pessimistic model: exact lower-equilibrium reformulation (MF)

For each $x \in X$ the pessimistic leader value is generated exactly by the lower-level GNEP

$$\text{Player 1: } \min_y -F(x, y) \quad \text{s.t. } y \in Y, f(x, y) \leq f(x, v) + \epsilon, \quad (MF)$$

$$\text{Player 2: } \min_v f(x, v) \quad \text{s.t. } v \in Y.$$

At equilibrium, $f(x, v^*) = \phi(x)$, and $F(x, y^*) = \psi_\epsilon^p(x)$. The pessimistic bilevel problem is therefore $\min_{x \in X} \psi_\epsilon^p(x)$ [39].

KKT system. With multiplier $\lambda \geq 0$ on player 1's coupling constraint and nothing on player 2 (which sees only $v \in Y$):

$$0 \in -\nabla_y F(x, y) + \lambda \nabla_y f(x, y) + N_Y(y), \quad (22)$$

$$0 \in \nabla_v f(x, v) + N_Y(v), \quad (23)$$

$$0 \leq \lambda \perp f(x, y) - f(x, v) - \epsilon \leq 0. \quad (24)$$

Note that in (22), player 1 sees x as fixed, so only $\nabla_y f(x, y)$ appears in the coupling-constraint gradient; no $-\nabla_y f(x, v)$ term is present because v belongs to player 2, not player 1.

Nikaido–Isoda gap function. An alternative characterization useful for computation [40, 41, 60, 62] is the Nikaido–Isoda gap function

$$\begin{aligned} \mathcal{N}_x(y, v) := & \sup_{\hat{y} \in Y: f(x, \hat{y}) \leq f(x, v) + \epsilon} [F(x, \hat{y}) - F(x, y)] \\ & + \sup_{\hat{v} \in Y} [f(x, v) - f(x, \hat{v})]. \end{aligned} \quad (25)$$

Then (y, v) solves (MF) iff $\mathcal{N}_x(y, v) = 0$, and $F(x, y) = \psi_\epsilon^p(x)$. We use this formulation computationally in Section 5 to give teeth to the claim that the pessimistic reformulation is doing real work.

We summarize the distinct computational roles that the three reformulations play in Table 1.

Table 1: Computational roles of the three GNEP reformulations.

Reformulation	Role	Use in this paper
(G1)	Global-solution analysis	Conceptual; not used directly for computation.
(G2)	Stationarity, algorithm design	Proximal alternating scheme (§5.1).
(MF)	Worst-case implementation	NI-gap penalization (§5.2).

5 Computational Workflow

This section specifies the concrete computational procedures used in the case studies. We use (G2) computationally for the optimistic side (§5.1) and a Nikaido–Isoda penalization of (MF) for the pessimistic side (§5.2). The frontier is constructed by a structured scalarization sweep over weights.

5.1 Optimistic candidate generation via proximal alternating linearization

Let (x^k, y^k, v^k) denote the current iterate with $v^k \in S(x^k)$. Given $\tau_k > 0$, the updated leader–follower pair solves the proximal subproblem

$$(x^{k+1}, y^{k+1}) \in \arg \min_{(x, y) \in \mathcal{K}(x^k, v^k)} \left\{ F(x, y) + \frac{\tau_k}{2} \|x - x^k\|^2 + \frac{\tau_k}{2} \|y - y^k\|^2 \right\}, \quad (26)$$

where

$$\mathcal{K}(x^k, v^k) := \{(x, y) \in X \times Y : f(x, y) \leq f(x^k, v^k) + \nabla_1 f(x^k, v^k)^\top (x - x^k) + \epsilon\}. \quad (27)$$

The follower update is $v^{k+1} \in \arg \min_{v \in Y} f(x^{k+1}, v)$.

The stopping test is $\max\{\|z^{k+1} - z^k\|, r_{\text{LL}}^\epsilon(x^k, y^k), g_{\text{stat}}^\epsilon(x^k, y^k, v^k, \lambda^k)\} \leq \text{tol}$, where $z^k = (x^k, y^k)$ and the stationarity residual uses the Fischer–Burmeister form of the GNEP KKT system (28). Under the assumptions required by the convexified GNEP reformulation of Lampariello and Sagratella [38]—which include fully convex lower-level objective, appropriate constraint qualifications, and algorithm-specific conditions that we do not verify in full for the case studies—this type of stationarity-oriented scheme targets stationary points of the optimistic problem. We use it here as a computational heuristic rather than as a globally convergent algorithm, and we label outputs accordingly.

Stationarity residual, formal definition. The stationarity residual $g_{\text{stat}}^\epsilon(x, y, v, \lambda)$ used in the stopping test is defined through the GNEP KKT system (18)–(21). Using the Fischer–Burmeister function $\varphi_{\text{FB}}(a, b) := a + b - \sqrt{a^2 + b^2}$, which satisfies $\varphi_{\text{FB}}(a, b) = 0 \iff a \geq 0, b \geq 0, ab = 0$ [42, 43], and the natural-residual projections $R_X(z, w) := z - \text{proj}_X(z - w)$ and R_Y analogously, we define

$$\begin{aligned} g_{\text{stat}}^\epsilon(x, y, v, \lambda)^2 := & \|R_X(x, \nabla_x F(x, y) + \lambda(\nabla_x f(x, y) - \nabla_x f(x, v)))\|^2 \\ & + \|R_Y(y, \nabla_y F(x, y) + \lambda \nabla_y f(x, y))\|^2 \\ & + \|R_Y(v, \nabla_v f(x, v))\|^2 \\ & + \varphi_{\text{FB}}(\lambda, -[f(x, y) - f(x, v) - \epsilon])^2. \end{aligned} \quad (28)$$

This quantity uses only first derivatives of F and f and requires no derivative of ϕ . It is evaluated at the multiplier $\lambda \geq 0$ returned by the proximal subproblem solver without the optimization over λ .

5.2 Pessimistic evaluation via NI-gap penalization

For a candidate decision $x \in X$, we evaluate $\psi_\epsilon^p(x)$ by applying a penalty to the Nikaido–Isoda gap (25). This is the concrete computational role of the lower-equilibrium reformulation.

Inner evaluation. Fix x . For a penalty $\sigma > 0$, compute

$$(y^\sigma, v^\sigma) \in \arg \min_{y \in Y, v \in Y} \left\{ -F(x, y) + \sigma \cdot [\mathcal{N}_x(y, v)]_+ \right\}, \quad (29)$$

where $[\cdot]_+$ denotes nonnegative truncation (included for numerical safety, since $\mathcal{N}_x(y, v) \geq 0$ throughout). In the compact setting, exact global minimization of $-F(x, y) + \sigma \mathcal{N}_x(y, v)$ along a schedule $\sigma_t \uparrow \infty$ yields accumulation points with vanishing NI gap under standard penalty arguments [41, 60, 62], so that $F(x, y^\sigma) \rightarrow \psi_\epsilon^p(x)$. In our numerical experiments, however, the penalized subproblems are nonconvex and are solved locally with SLSQP from multiple starts; the reported pessimistic values should therefore be interpreted as certified only by the achieved NI gaps and status labels, not as global pessimistic values. We use $\sigma \in \{10^1, 10^2, 10^3, 10^4\}$ and stop when \mathcal{N}_x falls below 10^{-6} ; the achieved gap is reported alongside each pessimistic evaluation in the supplementary code.

Outer search. To solve $\min_{x \in X} \psi_\epsilon^p(x)$, we combine the NI-gap inner evaluation with a derivative-free outer search using multistart Powell / Nelder–Mead, as in [63, 64]. We report multistart counts, starting points, and status labels with the results.

5.3 Frontier construction via scalarization sweep

For each weight $\omega \in [0, 1]$ define the scalarized leader problem

$$\min_{x \in X} \left\{ (1 - \omega) \psi_\epsilon^o(x) + \omega \Delta_\epsilon(x) \right\}. \quad (30)$$

Let ω range over a deterministic grid $\omega_j = j/(J - 1)$, $j = 0, \dots, J - 1$. Each subproblem (30) is solved by a black-box multistart procedure, with inner evaluations of ψ_ϵ^o and ψ_ϵ^p as above. The weighted-sum sweep recovers *supported* nondominated points, i.e. points on the convex hull of the attainable objective set [65, 66]. In nonconvex objective images, it need not recover unsupported portions of the frontier, which motivates the Latin-hypercube fill of N_{LHS} additional samples. Compared to unstructured uniform sampling, this design covers the supported frontier explicitly through the ω -grid and fills the interior more efficiently [67, 68].

Status labels. Consistent with standard computational reporting conventions [69, 70], we label outputs as *converged*, *incumbent*, *heuristic*, or *empirical Pareto*. Only *converged* outputs have passed the full stopping test; *incumbents* are returned at iteration limits; *heuristic* denotes manually specified benchmarks; *empirical Pareto* denotes undominated points within the sampled candidate set.

5.4 Assumptions used where

Because the paper moves between compactness, Lipschitz continuity, quadratic growth, differentiability, convexity, and GNEP stationarity, Table 2 maps each result to the assumptions it requires. The standing assumptions (Assumption 2.1: X, Y compact and F, f continuous) are used throughout; additional assumptions are introduced only where they are needed.

Table 2: Map of assumptions to results.

Result	Main assumptions	Purpose
Prop. 3.1	Standing (compactness, continuity)	Attainment of ψ^o, ψ^p ; one-dim. diameter form.
Prop. 3.2	Standing	Monotonicity in ϵ .
Thm. 3.3	Standing; $F(x, \cdot)$ Lipschitz on Y with modulus $L_F(x)$	Diameter-based bound.
Cor. 3.5	Above plus quadratic lower-level growth (Ass. 3.4)	$O(\sqrt{\epsilon})$ rate.
Eq. (16)–(17)	Standing; f twice continuously differentiable; second-order sufficient condition at $y^*(x)$; $S(x)$ singleton	Directional expansion.
Prop. 3.8, semicontinuity part	Standing	USC of S_ϵ , USC of ψ^p , LSC of ψ^o .
Prop. 3.8, continuity part	Above plus correspondence continuity of S_ϵ at (x_0, ϵ_0)	Continuity of $\psi^o, \psi^p, \Delta_\epsilon$.
GNEP KKT systems (18)–(21), (22)–(24)	F, f continuously differentiable; appropriate constraint qualifications	First-order conditions.
Stationarity residual (28)	Continuous differentiability of F, f on a neighborhood of the candidate point	Computational diagnostic.
Proximal scheme (26)	Convexity assumptions of [38] (full lower-level convexity, CQ, etc.)	Stationarity-targeting heuristic.
NI penalization (29)	Compactness; exact global minimization (theory) / local SLSQP (practice)	Pessimistic evaluation.

6 Case Study 1: Stackelberg Pricing on a Parallel-Link Network with Genuine Follower Multiplicity

This case study is designed to exercise the diagnostic on an instance where the follower’s optimal response is genuinely set-valued along a positive-dimensional, codimension-one indifference subset of the leader’s decision region. It is deliberately small, so that all quantities can be written down in closed form and the framework can be compared against exact values.

6.1 Model

A planner sets tolls $x = (x_1, x_2) \in X := [0, 2]^2$ on two parallel links between a single origin-destination pair with unit demand. Link i has an access cost a_i ; we use $a = (1.0, 1.2)$. A representative user chooses flow split $y = (y_1, y_2) \in Y$ with

$$Y := \{y \in \mathbb{R}_+^2 : y_1 + y_2 = 1\}, \quad (31)$$

and minimizes the linear travel cost

$$f(x, y) := (a_1 + x_1)y_1 + (a_2 + x_2)y_2. \quad (32)$$

When $a_1 + x_1 \neq a_2 + x_2$, the follower's optimum is the unique unit mass on the cheaper link; when $a_1 + x_1 = a_2 + x_2$, every $y \in Y$ is optimal. Thus the follower's exact optimal set is

$$S(x) = \begin{cases} \{(1, 0)\} & \text{if } a_1 + x_1 < a_2 + x_2, \\ \{(0, 1)\} & \text{if } a_1 + x_1 > a_2 + x_2, \\ Y & \text{if } a_1 + x_1 = a_2 + x_2. \end{cases} \quad (33)$$

Along the indifference line $\mathcal{L} := \{x \in X : x_2 = x_1 - 0.2\}$, the follower's exact optimum is an entire line segment.

The planner has a system-cost objective that balances congestion and revenue:

$$F(x, y) := c_1 y_1^2 + c_2 y_2^2 - \alpha (x_1 y_1 + x_2 y_2) + \beta (x_1^2 + x_2^2). \quad (34)$$

We use $c_1 = 1.5$, $c_2 = 1.0$, $\alpha = 0.3$, $\beta = 0.05$. The term $c_1 y_1^2 + c_2 y_2^2$ is a stylized quadratic congestion cost, $\alpha(x \cdot y)$ is toll revenue valued by the planner, and $\beta \|x\|^2$ discourages extreme tolls. Both X and Y are compact; F is quadratic and f is linear, so Assumptions 2.1 and the Lipschitz condition on $F(x, \cdot)$ are satisfied.

6.2 Explicit ambiguity premium

Along \mathcal{L} the set $S(x) = Y$ is the whole simplex, so

$$\Delta_0(x) = \max_{y \in Y} F(x, y) - \min_{y \in Y} F(x, y) \quad \text{for } x \in \mathcal{L}. \quad (35)$$

With unit demand, parameterize $y = (t, 1 - t)$ for $t \in [0, 1]$. The leader's objective on Y for $x \in \mathcal{L}$ is

$$F(x, (t, 1 - t)) = c_1 t^2 + c_2 (1 - t)^2 - \alpha [x_1 t + x_2 (1 - t)] + \beta \|x\|^2, \quad (36)$$

a strictly convex quadratic in t . Expanding,

$$F(x, (t, 1 - t)) = (c_1 + c_2) t^2 + [-2c_2 - \alpha(x_1 - x_2)] t + \text{const}(x), \quad (37)$$

where $\text{const}(x) = c_2 - \alpha x_2 + \beta \|x\|^2$. The first-order condition $\partial_t F = 0$ reads $2(c_1 + c_2)t - 2c_2 - \alpha(x_1 - x_2) = 0$, so the unconstrained interior minimizer is

$$t^*(x) = \frac{2c_2 + \alpha(x_1 - x_2)}{2(c_1 + c_2)} = \frac{c_2 + \frac{1}{2}\alpha(x_1 - x_2)}{c_1 + c_2}, \quad (38)$$

clipped to $[0, 1]$; the right-hand equality is the form used in the supplementary code, obtained by dividing numerator and denominator by 2. The maximum of the strictly convex quadratic on $[0, 1]$

is attained at an endpoint $t \in \{0, 1\}$. For the nominal-optimal point $x = (1.6, 1.4) \in \mathcal{L}$, which minimizes ψ_0^o on $\mathcal{L} \cap X$, (38) gives $t^* = (2 \cdot 1.0 + 0.3 \cdot 0.2)/(2 \cdot 2.5) = 2.06/5.0 = 0.412$, and the pessimistic maximum is attained at $t = 0$, giving

$$\Delta_0((1.6, 1.4)) = F((1.6, 1.4), (1, 0)) - F((1.6, 1.4), (0.412, 0.588)) \approx 0.864, \quad (39)$$

a large, strictly positive ambiguity premium at exact follower optimality. Off \mathcal{L} , the exact $S(x)$ is a singleton and $\Delta_0(x) = 0$.

6.3 ϵ -neighborhood and the full framework

For $\epsilon > 0$, whether on or off \mathcal{L} , the set $S_\epsilon(x)$ is characterized explicitly. If $a_1 + x_1 < a_2 + x_2$, writing $\delta(x) := (a_2 + x_2) - (a_1 + x_1) > 0$, one has

$$S_\epsilon(x) = \{y = (1 - s, s) : s \in [0, \min(1, \epsilon/\delta(x))]\}. \quad (40)$$

This allows one to compute ψ_ϵ^o , ψ_ϵ^p , and Δ_ϵ in closed form along any ray in X . We use $\epsilon = 0.10$ in the main reported run.

6.4 Scalarization sweep and frontier

We solve (30) for $J = 21$ weights $\omega_j = j/20$, $j = 0, \dots, 20$, augmented with $N_{\text{LHS}} = 80$ Latin-hypercube samples on X . Table 3 reports diagnostics at seven representative points: five scalarization snapshots ($\omega \in \{0, 0.25, 0.5, 0.75, 1\}$), and two heuristic benchmarks. Values are computed in closed form from (36)–(40) and verified by the supplementary code.

Table 3: Case Study 1 diagnostics at representative leader decisions, $\epsilon = 0.10$. All values in model units. “ ω ” denotes the scalarization weight. “On \mathcal{L} ” indicates whether x satisfies $x_2 = x_1 - 0.2$.

Label	x_1	x_2	On \mathcal{L}	$\psi_\epsilon^o(x)$	$\Delta_\epsilon(x)$	$\rho_\epsilon(x)$
$\omega = 0$ (nominal, on \mathcal{L})	1.60	1.40	yes	0.382	0.864	0.626
$\omega = 0.25$	1.60	1.20	no	0.391	0.449	0.323
$\omega = 0.5$	1.60	1.00	no	0.489	0.389	0.261
$\omega = 0.75$	1.60	0.50	no	0.762	0.228	0.129
$\omega = 1$ (robust corner)	2.00	0.00	no	1.063	0.137	0.066
Heur. no toll	0.00	0.00	no	0.625	0.875	0.538
Heur. symmetric	1.00	1.00	no	0.425	0.875	0.614

The key qualitative phenomena are visible in Table 3. First, the nominal-optimal policy sits on the indifference line \mathcal{L} and has the smallest ψ_ϵ^o of the set (0.382) but a large ambiguity premium (0.864) driven by genuine follower multiplicity. Second, moving the leader’s second toll x_2 away from the indifference value $x_1 - 0.2$ trades nominal efficiency for robustness in a continuous way: as x_2 decreases from 1.40 to 0.00 along the ω -sweep, ψ_ϵ^o rises from 0.382 to 1.063 while Δ_ϵ falls from 0.864 to 0.137. Third, at both heuristic benchmarks the cost gap is $\delta = 0.2$, so with $\epsilon = 0.10$ the admissible parameter range is $s \in [0, \epsilon/\delta] = [0, 0.5]$, i.e. a *half*-simplex of flow splits. Directly computing ψ_ϵ^o and ψ_ϵ^p on this half-simplex yields $\Delta_\epsilon = 0.875$ at both $(0, 0)$ and $(1, 1)$ —a substantial ambiguity that is only partially absorbed by the codimension-one geometry of \mathcal{L} . This is precisely the phenomenon the diagnostic is designed to surface.

Figure 1 displays the computed robustness–efficiency frontier in the $(\psi_\epsilon^o, \Delta_\epsilon)$ plane. The scalarization sweep populates a well-resolved curve, with the nominal corner on \mathcal{L} , the robust corner off \mathcal{L} , and a dense collection of compromise points in between. The supported points form a smooth decreasing trade-off curve, reflecting the classical efficiency–robustness tension.

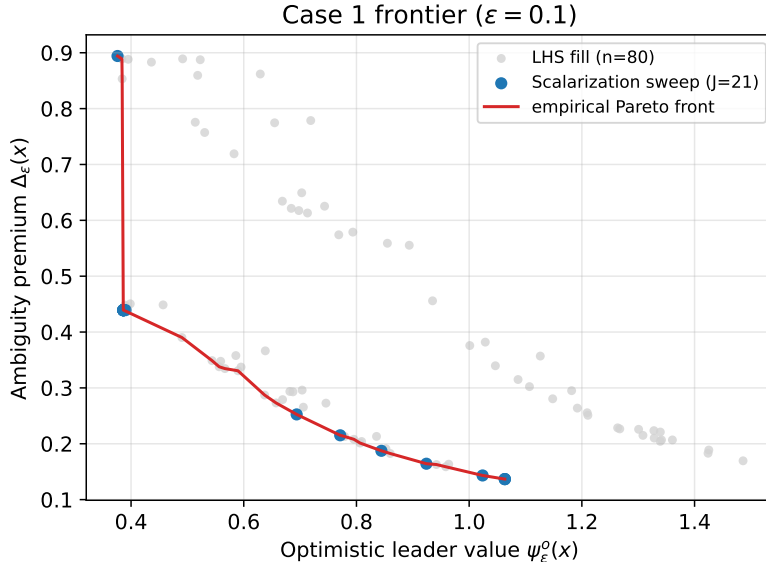


Figure 1: Robustness–efficiency frontier for Case Study 1 ($\epsilon = 0.10$). Blue dots: scalarization sweep over 21 weights. Gray dots: 80 Latin-hypercube samples. The nominal-optimal corner lies on the indifference line \mathcal{L} ; the robustness-optimal corner lies strictly off \mathcal{L} .

6.5 Interpretation

Case Study 1 demonstrates the framework in the mode it was motivated to serve: a Stackelberg game with a follower whose best response is genuinely set-valued along a positive-dimensional, codimension-one indifference subset of the leader’s decision region. Here the ambiguity premium $\Delta_\epsilon(x)$ is not a stability artifact but a real feature of the follower’s optimal correspondence, and the robustness–efficiency frontier displays both regimes—a high-reward brittle corner and a safer interior—with intermediate compromise policies populating the curve.

7 Case Study 2: Convex Generation-Capacity Planning with Reliability-Type Diversification Constraints

Building on the stylized convex generation-planning model, this second case study introduces reliability-motivated diversification constraints to rule out unrealistic single-technology portfolios. Methodologically, we use the structured scalarization sweep of §5.3 rather than unstructured uniform random sampling. Furthermore, rather than focusing on prescriptive managerial claims, this section is specifically designed to illustrate how the framework behaves when multiplicity is absent and ambiguity arises only from the ϵ -relaxation, consistent with Corollary 3.5.

7.1 Model

We use a four-technology planning model with utility-scale solar photovoltaics, onshore wind, natural-gas combined cycle, and a stylized four-hour battery-like flexibility resource. The technology data follow the open NREL ATB conventions and are reported in Table 4 for transparency; quantitative values should not be interpreted as empirical forecasts.

Table 4: Stylized technology data. Annualized capital assumes 7% discount rate, 25-year life.

Technology	CAPEX (\$/kW)	Ann. cap. (\$B/GW-yr)	Var. cost (\$/MWh)	Cap. factor
Solar PV	1,194	0.1025	5.0	0.246
Onshore Wind	1,462	0.1255	7.0	0.345
Gas CCGT	958	0.0822	28.6	0.870
Battery 4h	1,247	0.1070	8.2	0.200

Leader and follower. Leader variables $x = (x_1, \dots, x_4)$ are installed capacities in GW; follower variables $y = (y_1, \dots, y_4)$ are average dispatches in GW. Following the standing framework, the leader’s effective feasible set is a fixed compact subset of \mathbb{R}^4 , and the follower’s feasible set Y is a fixed compact box independent of x :

$$\begin{aligned} X_{\text{box}} &:= [0.2, 8.0] \times [0.2, 6.0] \times [0.5, 10.0] \times [0.1, 4.0], \\ Y &:= [0, 6.0] \times [0, 5.0] \times [0, 9.0] \times [0, 3.5]. \end{aligned} \quad (41)$$

The dispatch box Y is sized generously so that the unconstrained per-technology optimal dispatch $y_i = \alpha_i x_i$ is interior to Y for every $x \in X_{\text{box}}$ used in the case study. The coupling between capacities and dispatches enters *soft*, through the lower-level objective’s penalization of $|y_i - \alpha_i x_i|$, rather than through a feasibility restriction $y_i \leq x_i$; this keeps Y leader-independent and preserves the standing assumptions of Section 2.

Lower-level objective

$$f(x, y) = \sum_i w_i (y_i - \alpha_i x_i)^2 + \mu_D \left(\sum_i y_i - D \right)^2, \quad (42)$$

with $\alpha = (0.246, 0.345, 0.870, 0.200)$, $w = (3.0, 2.5, 1.0, 2.0)$, $\mu_D = 2.0$, and $D = 5.0$ GW.

Leader objective

$$F(x, y) = \sum_i \kappa_i x_i + \sum_i \beta_i (x_i - y_i)^2 + \sum_i \tilde{c}_i y_i + \lambda_D \left(\sum_i y_i - D \right)^2, \quad (43)$$

with κ from Table 4, $\beta = (0.15, 0.12, 0.05, 0.08)$, \tilde{c}_i annualized dispatch-cost coefficients, and $\lambda_D = 1.5$.

Reliability-type diversification constraints. We add the constraints

$$\sum_i x_i \geq D, \quad x_i \leq 0.6 \sum_j x_j \quad \forall i, \quad x_i \geq \underline{x}_i \text{ (min build)}, \quad (44)$$

with $\underline{x} = (0.2, 0.2, 0.5, 0.1)$ GW. The first constraint enforces nameplate adequacy; the second caps any single technology’s share below 60%, a stylized diversification criterion consistent with planning practice in many jurisdictions [71–75]; the third prevents zero build of any technology. These constraints preclude the trivial all-gas corner reported in the earlier version and make the robustness–efficiency trade-off nontrivial. The effective leader feasible set is therefore

$$X_{\text{feas}} := \left\{ x \in X_{\text{box}} : \sum_i x_i \geq D, \quad x_i \leq 0.6 \sum_j x_j \quad \forall i \right\}, \quad (45)$$

which is a closed compact subset of \mathbb{R}^4 . In the notation of Sections 2–5, we take $X = X_{\text{feas}}$ throughout this case study.

Follower uniqueness. Because (42) is strictly convex in y , $S(x)$ is a singleton for every x . By Corollary 3.5, the ambiguity premium satisfies $\Delta_\epsilon(x) \leq 2L_F(x)\sqrt{\epsilon/\mu(x)}$. A valid quadratic-growth constant under the convention of Assumption 3.4 (the inequality $f(x, y) - \phi(x) \geq \mu(x) \text{dist}(y, S(x))^2$, not Hessian strong-convexity) is $\mu(x) = \min_i w_i = 1.0$. The case study therefore illustrates the framework in the regime where multiplicity is absent and ambiguity arises from $\epsilon > 0$, exactly as the theory predicts.

7.2 Results

We use the workflow of Section 5 to compute a candidate nominal optimum (which solves $\min_{x \in X_{\text{feas}}} \psi_\epsilon^o(x)$ by multistart Powell with NI-penalized inner pessimistic evaluation), a candidate robust optimum (which solves $\min_{x \in X_{\text{feas}}} \Delta_\epsilon(x)$ similarly), and a family of convex-combination intermediates along the segment between them. Latin-hypercube samples ($N_{\text{LHS}} = 80$) populate the interior of the feasible region. The sweep-plus-fill design produces the frontier in Figure 2. Table 5 reports diagnostics at seven representative policies. We explicitly note that $\psi_\epsilon^o(x)$ is a function of x , so entries in the ψ^o column are evaluations of the same leader functional at different portfolios, not competing values of a single optimization.

Table 5: Case Study 2 diagnostics at representative policies, $\epsilon = 0.5$. Diversification constraints active (share cap 0.6, reserve margin $\sum x_i \geq D = 5$, minimum builds). Capacities x in GW; cost units \$B/yr. The “status” column labels the computational provenance: *incumbent* denotes the best multistart solution for the indicated objective, and *convex comb.* denotes a policy on the line segment between the two incumbents.

Label	x_1	x_2	x_3	x_4	ψ^o	Δ	ρ	Status
Solver incumbent for nominal solve	1.09	0.35	2.58	0.98	0.599	1.129	0.706	incumbent
Convex comb. $t=0.25$	1.08	0.54	3.18	1.03	0.681	0.900	0.535	convex comb.
Convex comb. $t=0.50$	1.08	0.72	3.79	1.08	0.799	0.695	0.387	convex comb.
Convex comb. $t=0.75$	1.07	0.91	4.39	1.12	0.949	0.518	0.266	convex comb.
Solver incumbent for robust solve	1.06	1.09	4.99	1.17	1.132	0.370	0.174	incumbent
Heur. gas-heavy (cap-binding)	0.79	0.79	3.12	0.50	0.596	0.922	0.578	heuristic
Heur. renewables-heavy	3.00	2.50	1.00	0.50	1.451	1.460	0.596	heuristic

Table 5 illustrates several phenomena worth highlighting. First, among the scalarization-generated sweep points, the solver incumbent for the nominal solve has the second smallest ψ^o and the second largest Δ , whereas the solver incumbent for the robust solve has the second largest ψ^o and the smallest Δ ; the convex-combination intermediates trace out a monotone trade-off.

Second, Table 5 also illustrates the diagnostic value of reporting sampled heuristics alongside solver incumbents. The gas-heavy heuristic slightly improves on the reported solver incumbent for the nominal solve in both displayed criteria, with $(\psi^o, \Delta) = (0.596, 0.922)$ compared with $(0.599, 1.129)$. Thus, within the sampled set, the solver incumbent is not empirically nondominated. We keep both rows in the table to make the computational status transparent: the “solver incumbent” is the best multistart output for the nominal solve, whereas the heuristic is a hand-specified benchmark that exposes a missed or weak local solution. This reinforces the paper’s diagnostic stance and motivates reporting status labels rather than presenting the multistart outputs as certified global optima.

Third, the 60% share cap binds at the solver incumbent for the robust solve ($x_3/\sum_j x_j = 4.99/8.31 \approx 0.600$) and at the gas-heavy heuristic ($3.12/5.20 = 0.600$), but not at the solver incumbent for the nominal solve (gas share $2.58/5.00 \approx 0.516$) nor at the renewables-heavy heuristic

(largest share ≈ 0.429 in solar). No portfolio degenerates to a single-technology corner, and the constraint is tight where one would expect: in the gas-dominated regime corresponding to high robustness in this stylized model.

The $O(\sqrt{\epsilon})$ prediction of Corollary 3.5 is examined empirically in Figure 3, which plots the ratio $\Delta_\epsilon(x)/\sqrt{\epsilon}$ at the balanced policy $x = (1.08, 0.72, 3.79, 1.08)$ for $\epsilon \in \{0.05, 0.1, 0.25, 0.5, 1, 2, 4\}$. The computed ratios are 0.810, 0.830, 0.892, 0.983, 1.129, 1.351, 1.688. The ratio is relatively stable for small ϵ and rises for larger tolerances, consistent with a leading-order $\sqrt{\epsilon}$ effect plus higher-order corrections that become non-negligible as ϵ approaches unity in problem units.

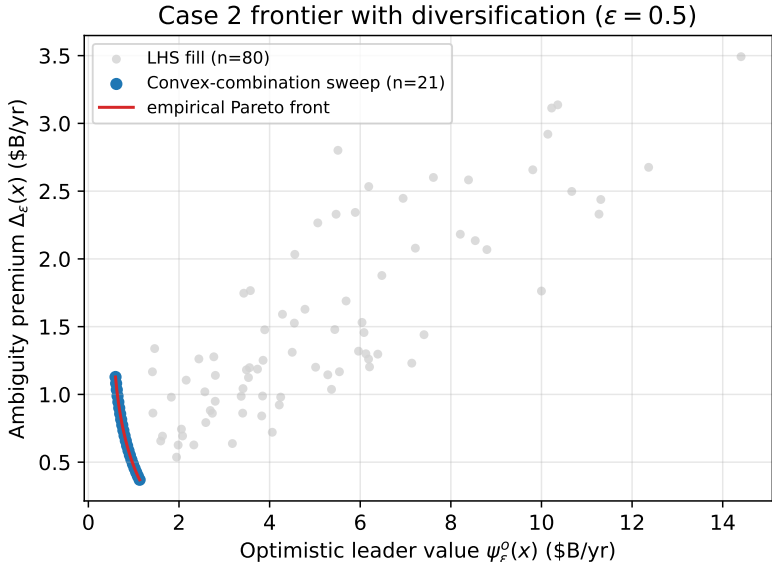


Figure 2: Robustness–efficiency frontier for Case Study 2 ($\epsilon = 0.5$), with diversification constraints. Blue dots: scalarization sweep. Gray dots: Latin-hypercube fill.

7.3 Interpretation

The generation-planning example illustrates a different regime from Case Study 1. The lower-level problem is strictly convex, so exact follower multiplicity is absent. Any ambiguity premium therefore comes from the ϵ -optimal response set rather than from multiple exact optima. The purpose of the example is to show how the diagnostic behaves when implementation slack, rather than exact multiplicity, is the source of exposure.

With diversification constraints in place, no portfolio degenerates to a single-technology corner. The multistart workflow identifies a solver incumbent for the nominal solve with a gas-heavy but not share-cap-binding mix—roughly 2.58 GW CCGT out of a 5.00 GW total, with gas accounting for about 52% of total capacity—and a solver incumbent for the robust solve that increases total capacity substantially (to about 8.31 GW) and pushes the gas share to the diversification cap ($\approx 60\%$), while also increasing wind and battery capacity in absolute terms relative to the nominal solver incumbent. We do not claim that either is the right investment recommendation for any real system. What we claim is only that:

1. even without follower multiplicity, the ambiguity premium is strictly positive because the ϵ -response set has positive diameter (Corollary 3.5);

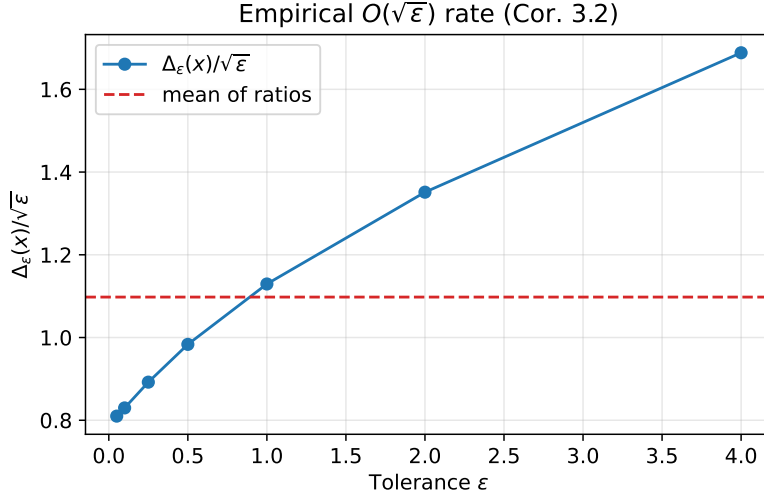


Figure 3: Empirical check of the $O(\sqrt{\epsilon})$ rate (Corollary 3.5): ratio $\Delta_\epsilon/\sqrt{\epsilon}$ for the balanced policy across a grid of ϵ . The ratio is relatively stable for small ϵ and rises for larger tolerances, consistent with a leading-order $\sqrt{\epsilon}$ effect plus higher-order corrections.

2. the shape of the frontier is informative for screening, identifying policies that are nominally attractive but proportionally more exposed to near-optimal redispatch;
3. the framework is sensitive to the choice of diversification or reliability constraints. Without such constraints, the earlier all-gas pessimistic solution we documented in a preliminary version of this paper was an artifact of the model’s omission of reliability and contingency dimensions, not a substantive recommendation.

This illustrates a general point: the ambiguity premium is one dimension of robustness among several (contingency, outage, uncertainty). A well-posed planning problem must combine it with the dimensions captured by standard reliability and uncertainty-aware planning models [76–78].

8 Managerial Insights

The diagnostic framework supports decision-makers in three concrete ways. First, by reporting each candidate decision as a triple $(\psi_\epsilon^o(x), \Delta_\epsilon(x), g_{\text{stat}}^\epsilon)$, it separates nominal efficiency, implementation robustness, and first-order computational quality that are often conflated in single-solution bilevel reports. Second, by visualizing the robustness–efficiency frontier generated via a structured scalarization sweep, it exposes whether a candidate decision sits on a brittle corner or a robust plateau. Third, by stress-testing $\Delta_\epsilon(x)$ across a grid of ϵ , it quantifies the sensitivity of a decision to implementation slack, forecast error, or near-optimal follower re-response.

As Case Study 2 illustrates, in models that omit reliability, outage, or network constraints, pessimistic optima can collapse to single-technology corners that minimize redispatch ambiguity only because the redispatch space itself has collapsed. The appropriate use of the framework is as a screening overlay on top of a planning model that is already well-posed with respect to the other dimensions of robustness a decision-maker cares about.

Within that scope, the framework applies naturally to network pricing and transportation [9, 10, 12], electricity market design [15, 18, 79, 80], Stackelberg investment and entry games [81], and regulatory decision-making in adversarial or strategic environments [19, 21, 82], as long as the analyst

is willing to treat it as one component of a larger decision-analytic process.

9 Discussion and Conclusion

We have proposed a diagnostic framework for hierarchical decision problems that organizes known optimistic and pessimistic bilevel–GNEP reformulations around the ambiguity premium $\Delta_\epsilon(x)$. The novelty is not the gap itself, which is classical, but the decision-analytic packaging around it: the Lipschitz-type bound relating $\Delta_\epsilon(x)$ to the diameter of the ϵ -response set, the $O(\sqrt{\epsilon})$ rate under quadratic lower-level growth, the structured scalarization sweep for frontier construction, and the combined use of the convexified optimistic reformulation and Nikaido–Isoda pessimistic evaluation as a screening workflow.

Several limitations should be noted. The stationarity residual (28) uses Fischer–Burmeister encoding, which is standard but in the presence of degenerate multipliers can fail to separate stationarity from numerical noise; more refined encodings are available [83–85]. The pessimistic outer solve is derivative-free multistart and does not return global certificates. The case studies are small and are chosen to expose the framework’s mechanics; scaling the Nikaido–Isoda penalization to high-dimensional problems is an area of active research [86].

Natural extensions include stochastic and robust lower-level models [30,44,45], network-constrained dispatch with unit-commitment multiplicity [87–89], and coupling with risk-averse leader objectives [90,91]. In all these directions the ambiguity premium can play the role of a compact diagnostic that exposes implementation risk that is otherwise easy to overlook.

A Proofs

Proof of Proposition 3.8. Upper semicontinuity of S_ϵ . Let $(x_k, \epsilon_k) \rightarrow (x, \epsilon)$ and let $y_k \in S_{\epsilon_k}(x_k)$ with $y_k \rightarrow y$. Since Y is compact, $y \in Y$. By continuity of f and ϕ ,

$$f(x, y) = \lim_{k \rightarrow \infty} f(x_k, y_k) \leq \lim_{k \rightarrow \infty} (\phi(x_k) + \epsilon_k) = \phi(x) + \epsilon.$$

Hence $y \in S_\epsilon(x)$. Therefore the graph of S_ϵ is closed. Since $S_\epsilon(x) \subseteq Y$ and Y is compact, each value $S_\epsilon(x)$ is compact and nonempty. Thus $(x, \epsilon) \mapsto S_\epsilon(x)$ is upper semicontinuous.

Semicontinuity of the marginal functions. Because S_ϵ is compact-valued and upper semicontinuous, Berge’s maximum theorem gives that

$$(x, \epsilon) \mapsto \psi_\epsilon^p(x) = \max_{y \in S_\epsilon(x)} F(x, y)$$

is upper semicontinuous and

$$(x, \epsilon) \mapsto \psi_\epsilon^o(x) = \min_{y \in S_\epsilon(x)} F(x, y)$$

is lower semicontinuous. Since $-\psi_\epsilon^o$ is upper semicontinuous, their difference

$$\Delta_\epsilon(x) = \psi_\epsilon^p(x) - \psi_\epsilon^o(x) = \psi_\epsilon^p(x) + (-\psi_\epsilon^o(x))$$

is upper semicontinuous as the sum of two upper semicontinuous functions.

Lower semicontinuity of S_ϵ at $(x_0, 0)$. Fix $y_0 \in S(x_0)$ and let $(x_k, \epsilon_k) \rightarrow (x_0, 0)$. Because $y_0 \in S(x_0)$, $f(x_0, y_0) = \phi(x_0)$. By continuity of f and ϕ , $f(x_k, y_0) - \phi(x_k) \rightarrow 0$. For all sufficiently large k , we have $x_k \in U$, so the quadratic growth condition yields

$$f(x_k, y_0) - \phi(x_k) \geq \underline{\mu} \operatorname{dist}(y_0, S(x_k))^2.$$

Therefore $\text{dist}(y_0, S(x_k)) \rightarrow 0$. Since $S(x_k)$ is nonempty and compact, there exists $\tilde{y}_k \in S(x_k)$ such that

$$\|\tilde{y}_k - y_0\| = \text{dist}(y_0, S(x_k)).$$

Hence $\tilde{y}_k \rightarrow y_0$. Moreover, $S(x_k) \subseteq S_{\epsilon_k}(x_k)$ because $\epsilon_k \geq 0$. Thus $\tilde{y}_k \in S_{\epsilon_k}(x_k)$ and $\tilde{y}_k \rightarrow y_0$, which proves lower semicontinuity of S_ϵ at $(x_0, 0)$.

Lower semicontinuity of S_ϵ at (x_0, ϵ_0) for $\epsilon_0 > 0$. Fix $y_0 \in S_{\epsilon_0}(x_0)$ and let $(x_k, \epsilon_k) \rightarrow (x_0, \epsilon_0)$.
If

$$f(x_0, y_0) < \phi(x_0) + \epsilon_0,$$

then by continuity of f and ϕ we have, for all sufficiently large k , $f(x_k, y_0) \leq \phi(x_k) + \epsilon_k$, so we may simply take $y_k := y_0$.

Now suppose

$$f(x_0, y_0) = \phi(x_0) + \epsilon_0.$$

Let $\hat{y} \in S(x_0)$, which exists by Assumption 2.1. For any $\alpha \in (0, 1)$, define

$$y_\alpha := (1 - \alpha)y_0 + \alpha\hat{y}.$$

Since Y is convex, $y_\alpha \in Y$. By convexity of $f(x_0, \cdot)$ on Y ,

$$f(x_0, y_\alpha) \leq (1 - \alpha)f(x_0, y_0) + \alpha f(x_0, \hat{y}) = (1 - \alpha)(\phi(x_0) + \epsilon_0) + \alpha\phi(x_0) = \phi(x_0) + (1 - \alpha)\epsilon_0 < \phi(x_0) + \epsilon_0.$$

Fix a sequence $\alpha_m \downarrow 0$. For each m , continuity again implies that there exists K_m such that for all $k \geq K_m$,

$$f(x_k, y_{\alpha_m}) \leq \phi(x_k) + \epsilon_k,$$

so $y_{\alpha_m} \in S_{\epsilon_k}(x_k)$. By choosing K_m strictly increasing and defining $y_k := y_{\alpha_m}$ for $K_m \leq k < K_{m+1}$, we obtain a sequence with $y_k \in S_{\epsilon_k}(x_k)$ and $y_k \rightarrow y_0$. This proves lower semicontinuity at (x_0, ϵ_0) .

Finally, when S_ϵ is both upper and lower semicontinuous at (x_0, ϵ_0) , Berge's maximum theorem implies that ψ_ϵ^o and ψ_ϵ^p are continuous at (x_0, ϵ_0) , and therefore so is $\Delta_\epsilon = \psi_\epsilon^p - \psi_\epsilon^o$. \square

Exactness of the Nikaido–Isoda penalization

This is standard [41, 60, 62] and is reproduced for self-containment. Fix $x \in X$. For any $(y, v) \in Y \times Y$, $\mathcal{N}_x(y, v) \geq 0$, with equality iff (y, v) is a lower equilibrium of the pessimistic GNEP (MF). By compactness of Y and continuity of the integrands, the suprema defining \mathcal{N}_x are attained. Continuity of \mathcal{N}_x follows under the standard continuity assumptions for the associated feasible correspondence; these are satisfied in the compact examples considered below and are standard in NI-gap penalty analyses [41, 62]. By compactness, for each $\sigma > 0$, (29) admits a minimizer (y^σ, v^σ) . Along any sequence $\sigma_t \uparrow \infty$, $\{(y^{\sigma_t}, v^{\sigma_t})\}$ is bounded; pass to a convergent subsequence with limit (y^*, v^*) .

Vanishing NI gap. Let (\bar{y}, \bar{v}) be a lower equilibrium attaining $\psi_\epsilon^p(x)$, which exists by compactness. Since $\mathcal{N}_x(\bar{y}, \bar{v}) = 0$, optimality of $(y^{\sigma_t}, v^{\sigma_t})$ for the penalized problem at σ_t gives

$$-F(x, y^{\sigma_t}) + \sigma_t \mathcal{N}_x(y^{\sigma_t}, v^{\sigma_t}) \leq -F(x, \bar{y}). \quad (46)$$

Rearranging (46),

$$\sigma_t \mathcal{N}_x(y^{\sigma_t}, v^{\sigma_t}) \leq F(x, y^{\sigma_t}) - F(x, \bar{y}) \leq \max_{y \in Y} F(x, y) - F(x, \bar{y}), \quad (47)$$

so the left-hand side is bounded above by a finite constant independent of t (continuity of F on the compact set Y ensures the maximum is finite). With $\sigma_t \uparrow \infty$, the inequality forces $\mathcal{N}_x(y^{\sigma_t}, v^{\sigma_t}) \rightarrow 0$ along the subsequence; by continuity of \mathcal{N}_x , $\mathcal{N}_x(y^*, v^*) = 0$, so (y^*, v^*) is a lower equilibrium of (MF).

Pessimistic optimality. Passing to the limit in (46) and using $\sigma_t \mathcal{N}_x(y^{\sigma_t}, v^{\sigma_t}) \geq 0$ together with continuity of F yields

$$-F(x, y^*) \leq -F(x, \bar{y}),$$

i.e. $F(x, y^*) \geq F(x, \bar{y}) = \psi_\epsilon^p(x)$. Conversely, since $\mathcal{N}_x(y^*, v^*) = 0$, the point y^* is an admissible pessimistic lower-level response (i.e. feasible for the inner pessimistic maximization defining $\psi_\epsilon^p(x)$), so $F(x, y^*) \leq \psi_\epsilon^p(x)$. Combining the two inequalities, $F(x, y^*) = \psi_\epsilon^p(x)$.

B Reproducibility

All computations were performed in Python using NumPy, SciPy, and Matplotlib. The supplementary code `reproduce.py` generates all tables and figures reported in the paper. The fixed seed `seed=7` is used for all Latin-hypercube samples.

Lower-level solves use SciPy’s SLSQP with `ftol=10-12`, `maxiter=500`.

Optimistic proximal scheme uses $\tau = 2.0$, max 120 iterations, tolerance 10^{-6} on the joint test.

Pessimistic NI-gap penalization uses $\sigma \in \{10, 10^2, 10^3, 10^4\}$ with SLSQP inner solves and multistart with $n_{\text{starts}} = 5$ in Case Study 1 and $n_{\text{starts}} = 8$ in Case Study 2.

Frontier sweep uses $J = 21$ weights and $N_{\text{LHS}} \in \{80, 120\}$ samples.

Status labels follow §5.3: *converged* (stopping test satisfied), *incumbent* (iteration limit reached), *heuristic* (hand-specified), *empirical Pareto* (undominated in sampled set).

References

- [1] Benoît Colson, Patrice Marcotte, and Gilles Savard. An overview of bilevel optimization. *Annals of operations research*, 153(1):235–256, 2007.
- [2] Zonghao Liu, Louis Shuo Wang, Jiguang Yu, Jilin Zhang, Erica Martel, and Shijia Li. Bidirectional endothelial feedback drives turing-vascular patterning and drug-resistance niches: a hybrid pde-agent-based study. *Bioengineering*, 12(10):1097, 2025.
- [3] Louis Shuo Wang and Jiguang Yu. Algebraic–spectral thresholds and discrete–continuous stability transfer in leslie–gower systems. *Electronic Research Archive*, 34(1):251–290, 2026.
- [4] Louis Shuo Wang, Jiguang Yu, Shijia Li, and Zonghao Liu. Analysis and mean-field limit of a hybrid pde-abm modeling angiogenesis-regulated resistance evolution. *Mathematics*, 13(17):2898, 2025.
- [5] Stephan Dempe. *Foundations of bilevel programming*. Springer, 2002.

- [6] Stephan Dempe and Alain Zemkoo. Bilevel optimization: Advances and next challenges, 2020.
- [7] Thomas Kleinert, Martine Labbé, Ivana Ljubić, and Martin Schmidt. A survey on mixed-integer programming techniques in bilevel optimization. *EURO Journal on Computational Optimization*, 9:100007, 2021.
- [8] Zhi-Quan Luo, Jong-Shi Pang, and Daniel Ralph. *Mathematical programs with equilibrium constraints*. Cambridge University Press, 1996.
- [9] Martine Labbé, Patrice Marcotte, and Gilles Savard. A bilevel model of taxation and its application to optimal highway pricing. *Management science*, 44(12-part-1):1608–1622, 1998.
- [10] Luce Brotcorne, Martine Labbé, Patrice Marcotte, and Gilles Savard. A bilevel model for toll optimization on a multicommodity transportation network. *Transportation science*, 35(4):345–358, 2001.
- [11] Stephan Dempe and Alain B Zemkoo. The bilevel programming problem: reformulations, constraint qualifications and optimality conditions. *Mathematical Programming*, 138(1):447–473, 2013.
- [12] François Gilbert, Patrice Marcotte, and Gilles Savard. A numerical study of the logit network pricing problem. *Transportation Science*, 49(3):706–719, 2015.
- [13] Jonathan F Bard. *Practical bilevel optimization: algorithms and applications*, volume 30. Springer Science & Business Media, 2013.
- [14] Zhongping Wan, Lijun Mao, and Guangmin Wang. Estimation of distribution algorithm for a class of nonlinear bilevel programming problems. *Information Sciences*, 256:184–196, 2014.
- [15] Steven A Gabriel, Antonio J Conejo, J David Fuller, Benjamin F Hobbs, and Carlos Ruiz. *Complementarity modeling in energy markets*. Springer Science & Business Media, 2012.
- [16] Louis Shuo Wang and Jiguang Yu. Analysis framework for stochastic predator–prey model with demographic noise. *Results in Applied Mathematics*, 27:100621, 2025.
- [17] Ye Liang, Louis Shuo Wang, Jiguang Yu, and Zonghao Liu. Global well-posedness and stability of nonlocal damage-structured lineage model with feedback and dedifferentiation. *Mathematics*, 13(22):3583, 2025.
- [18] Sonja Wogrin, Salvador Pineda, and Diego A Tejada-Arango. Applications of bilevel optimization in energy and electricity markets. In *Bilevel optimization: advances and next challenges*, pages 139–168. Springer, 2020.
- [19] J Cole Smith and Yongjia Song. A survey of network interdiction models and algorithms. *European Journal of Operational Research*, 283(3):797–811, 2020.
- [20] Louis Shuo Wang. Introduction to mathematical programming with equilibrium constraints (mpocs) and bilevel optimization. *arXiv preprint arXiv:2605.00386*, 2026.
- [21] Alberto Caprara, Margarida Carvalho, Andrea Lodi, and Gerhard J Woeginger. Bilevel knapsack with interdiction constraints. *INFORMS Journal on Computing*, 28(2):319–333, 2016.

- [22] Eitan Israeli and R Kevin Wood. Shortest-path network interdiction. *Networks: An International Journal*, 40(2):97–111, 2002.
- [23] Luca Franceschi, Paolo Frasconi, Saverio Salzo, Riccardo Grazzi, and Massimiliano Pontil. Bilevel programming for hyperparameter optimization and meta-learning. In *International conference on machine learning*, pages 1568–1577. PMLR, 2018.
- [24] Louis Shuo Wang, Jiguang Yu, and Zonghao Liu. A damage-structured pde model of stem cell hierarchies: The dual role of dedifferentiation in tissue homeostasis and aging. *Plos one*, 21(2):e0335163, 2026.
- [25] Risheng Liu, Jiaxin Gao, Jin Zhang, Deyu Meng, and Zhouchen Lin. Investigating bi-level optimization for learning and vision from a unified perspective: A survey and beyond. *IEEE Transactions on Pattern Analysis and Machine Intelligence*, 44(12):10045–10067, 2021.
- [26] Pierre Loridan and Jacqueline Morgan. Weak via strong stackelberg problem: new results. *Journal of global Optimization*, 8(3):263–287, 1996.
- [27] Jiguang Yu, Louis Shuo Wang, Zonghao Liu, and Jingfeng Liu. Pattern suppression and recovery under one-way versus two-way chemotactic coupling in hybrid partial differential equation–ordinary differential equation models. *Transport Phenomena*, (0), 2026.
- [28] Wolfram Wiesemann, Angelos Tsoukalas, Polyxeni-Margarita Kleniati, and Berç Rustem. Pessimistic bilevel optimization. *SIAM Journal on Optimization*, 23(1):353–380, 2013.
- [29] Zixin Wang, Danqing Wang, and Jiguang Yu. Multi-strategy hybrid improved intelligent algorithm for solving uav-mtsp. *Information Technology and Control*, 54(2):413–438, 2025.
- [30] Yasmine Beck, Ivana Ljubić, and Martin Schmidt. A survey on bilevel optimization under uncertainty. *European Journal of Operational Research*, 311(2):401–426, 2023.
- [31] Yuansheng Gao, Lei Li, and Jiguang Yu. Rolling prediction model of closing price based on eemd data noise reduction and hgs-delm. In *2022 International Conference on Data Analytics, Computing and Artificial Intelligence (ICDACAI)*, pages 255–260. IEEE, 2022.
- [32] Mathieu Besançon, Miguel F Anjos, and Luce Brotcorne. Near-optimal robust bilevel optimization. 2019.
- [33] Louis Shuo Wang. Lecture note for bounded controls in continuous-time and control of several variables. *arXiv preprint arXiv:2604.05882*, 2026.
- [34] Louis Shuo Wang. First-order optimality conditions for mathematical programming with equilibrium constraints. *arXiv preprint arXiv:2605.00388*, 2026.
- [35] Louis Shuo Wang. Introduction to exact penalization for mathematical programming with equilibrium constraints. *arXiv preprint arXiv:2605.00387*, 2026.
- [36] Francisco Facchinei and Christian Kanzow. Generalized nash equilibrium problems. *Annals of Operations Research*, 175(1):177–211, 2010.
- [37] Lorenzo Lampariello and Simone Sagratella. A bridge between bilevel programs and nash games. *Journal of Optimization Theory and Applications*, 174(2):613–635, 2017.

- [38] Lorenzo Lampariello and Simone Sagratella. Numerically tractable optimistic bilevel problems. *Computational Optimization and Applications*, 76(2):277–303, 2020.
- [39] Lorenzo Lampariello, Simone Sagratella, and Oliver Stein. The standard pessimistic bilevel problem. *SIAM Journal on Optimization*, 29(2):1634–1656, 2019.
- [40] Hukukane Nikaidô and Kazuo Isoda. Note on non-cooperative convex games. 1955.
- [41] Masao Fukushima. Equivalent differentiable optimization problems and descent methods for asymmetric variational inequality problems. *Mathematical programming*, 53(1):99–110, 1992.
- [42] Andreas Fischer. A special newton-type optimization method. *Optimization*, 24(3-4):269–284, 1992.
- [43] Francisco Facchinei and Jong-Shi Pang. *Finite-dimensional variational inequalities and complementarity problems*. Springer, 2003.
- [44] Christoph Buchheim, Dorothee Henke, and Jannik Iрмаi. The stochastic bilevel continuous knapsack problem with uncertain follower’s objective. *Journal of optimization theory and applications*, 194(2):521–542, 2022.
- [45] Johanna Burtscheidt, Matthias Claus, and Stephan Dempe. Risk-averse models in bilevel stochastic linear programming. *SIAM Journal on Optimization*, 30(1):377–406, 2020.
- [46] Polyxeni-M Kleniati and Claire S Adjiman. A generalization of the branch-and-sandwich algorithm: from continuous to mixed-integer nonlinear bilevel problems. *Computers & Chemical Engineering*, 72:373–386, 2015.
- [47] Hatim Djelassi, Alexander Mitsos, and Oliver Stein. Recent advances in nonconvex semi-infinite programming: Applications and algorithms. *EURO Journal on Computational Optimization*, 9:100006, 2021.
- [48] June Liu, Yuxin Fan, Zhong Chen, and Yue Zheng. Pessimistic bilevel optimization: a survey. *International Journal of Computational Intelligence Systems*, 11(1):725–736, 2018.
- [49] Alexander Mitsos, Panayiotis Lemonidis, and Paul I Barton. Global solution of bilevel programs with a nonconvex inner program. *Journal of Global Optimization*, 42(4):475–513, 2008.
- [50] Angelos Tsoukalas, Berç Rustem, and Efstratios N Pistikopoulos. A global optimization algorithm for generalized semi-infinite, continuous minimax with coupled constraints and bi-level problems. *Journal of Global Optimization*, 44(2):235–250, 2009.
- [51] Francisco Facchinei and Christian Kanzow. Generalized nash equilibrium problems. *4or*, 5(3):173–210, 2007.
- [52] Axel Dreves, Francisco Facchinei, Christian Kanzow, and Simone Sagratella. On the solution of the kkt conditions of generalized nash equilibrium problems. *SIAM Journal on Optimization*, 21(3):1082–1108, 2011.
- [53] Ankur A Kulkarni and Uday V Shanbhag. On the variational equilibrium as a refinement of the generalized nash equilibrium. *Automatica*, 48(1):45–55, 2012.
- [54] J Frédéric Bonnans and Alexander Shapiro. *Perturbation analysis of optimization problems*. Springer Science & Business Media, 2013.

- [55] Dmitriy Drusvyatskiy and Adrian S Lewis. Error bounds, quadratic growth, and linear convergence of proximal methods. *Mathematics of operations research*, 43(3):919–948, 2018.
- [56] Marian J Fabian, René Henrion, Alexander Y Kruger, and Jiří V Outrata. Error bounds: necessary and sufficient conditions. *Set-Valued and Variational Analysis*, 18(2):121–149, 2010.
- [57] Xiao-Dong Luo and Zhi-Quan Luo. Extension of hoffman’s error bound to polynomial systems. *SIAM Journal on Optimization*, 4(2):383–392, 1994.
- [58] Alexander Shapiro. Sensitivity analysis of nonlinear programs and differentiability properties of metric projections. *SIAM Journal on Control and Optimization*, 26(3):628–645, 1988.
- [59] Anthony V Fiacco. Introduction to sensitivity and stability analysis in non linear programming. 1983.
- [60] Patrick T Harker. Generalized nash games and quasi-variational inequalities. *European journal of Operational research*, 54(1):81–94, 1991.
- [61] Jong-Shi Pang and Masao Fukushima. Quasi-variational inequalities, generalized nash equilibria, and multi-leader-follower games. *Computational Management Science*, 2(1):21–56, 2005.
- [62] Anna Von Heusinger and Christian Kanzow. Optimization reformulations of the generalized nash equilibrium problem using nikaido-isoda-type functions. *Computational Optimization and Applications*, 43(3):353–377, 2009.
- [63] Andrew R Conn, Katya Scheinberg, and Luis N Vicente. *Introduction to derivative-free optimization*. SIAM, 2009.
- [64] Charles Audet and Warren Hare. *Derivative-free and blackbox optimization*, volume 1. Springer, 2017.
- [65] Matthias Ehrgott. *Multicriteria optimization*. Springer, 2005.
- [66] Kaisa Miettinen. *Nonlinear multiobjective optimization*, volume 12. Springer Science & Business Media, 1999.
- [67] Michael D McKay, Richard J Beckman, and William J Conover. A comparison of three methods for selecting values of input variables in the analysis of output from a computer code. *Technometrics*, 42(1):55–61, 2000.
- [68] Felipe AC Viana. A tutorial on latin hypercube design of experiments. *Quality and reliability engineering international*, 32(5):1975–1985, 2016.
- [69] Elizabeth D Dolan and Jorge J Moré. Benchmarking optimization software with performance profiles. *Mathematical programming*, 91(2):201–213, 2002.
- [70] Nicholas IM Gould, Dominique Orban, and Philippe L Toint. Cutest: a constrained and unconstrained testing environment with safe threads for mathematical optimization. *Computational optimization and applications*, 60(3):545–557, 2015.
- [71] S Kahrobaee and S Asgarpoor. Short and long-term reliability assessment of wind farms. In *North American Power Symposium 2010*, pages 1–6. IEEE, 2010.

- [72] Paul L Joskow. Comparing the costs of intermittent and dispatchable electricity generating technologies. *American Economic Review*, 101(3):238–241, 2011.
- [73] Farhad Billimoria and Rahmatallah Poudineh. Market design for resource adequacy: A reliability insurance overlay on energy-only electricity markets. *Utilities Policy*, 60:100935, 2019.
- [74] Alexander E MacDonald, Christopher TM Clack, Anneliese Alexander, Adam Dunbar, James Wilczak, and Yuanfu Xie. Future cost-competitive electricity systems and their impact on us co2 emissions. *Nature Climate Change*, 6(5):526–531, 2016.
- [75] Paul Denholm, Douglas J Arent, Samuel F Baldwin, Daniel E Bilello, Gregory L Brinkman, Jaquelin M Cochran, Wesley J Cole, Bethany Frew, Vahan Gevorgian, Jenny Heeter, et al. The challenges of achieving a 100% renewable electricity system in the united states. *Joule*, 5(6):1331–1352, 2021.
- [76] Antonio J Conejo, Miguel Carrión, Juan M Morales, et al. *Decision making under uncertainty in electricity markets*, volume 1. Springer, 2010.
- [77] John M Mulvey, Robert J Vanderbei, and Stavros A Zenios. Robust optimization of large-scale systems. *Operations research*, 43(2):264–281, 1995.
- [78] Erick Delage and Yinyu Ye. Distributionally robust optimization under moment uncertainty with application to data-driven problems. *Operations research*, 58(3):595–612, 2010.
- [79] Olivier Daxhelet and Yves Smeers. The eu regulation on cross-border trade of electricity: A two-stage equilibrium model. *European Journal of Operational Research*, 181(3):1396–1412, 2007.
- [80] Benjamin F Hobbs and Jong-Shi Pang. Nash-cournot equilibria in electric power markets with piecewise linear demand functions and joint constraints. *Operations Research*, 55(1):113–127, 2007.
- [81] Ekaterina Moiseeva, Mohammad Reza Hesamzadeh, and Darryl R Biggar. Exercise of market power on ramp rate in wind-integrated power systems. *IEEE Transactions on Power Systems*, 30(3):1614–1623, 2014.
- [82] Leonardo Lozano and J Cole Smith. A value-function-based exact approach for the bilevel mixed-integer programming problem. *Operations Research*, 65(3):768–786, 2017.
- [83] Christian Kanzow. Nonlinear complementarity as unconstrained optimization. *Journal of Optimization theory and applications*, 88(1):139–155, 1996.
- [84] Christian Kanzow and Helmut Kleinmichel. A new class of semismooth newton-type methods for nonlinear complementarity problems. *Computational Optimization and Applications*, 11(3):227–251, 1998.
- [85] Daniel Ralph and Stephan Dempe. Directional derivatives of the solution of a parametric nonlinear program. *Mathematical programming*, 70(1):159–172, 1995.
- [86] Axel Dreves and Nathan Sudermann-Merx. Solving linear generalized nash equilibrium problems numerically. *Optimization Methods and Software*, 31(5):1036–1063, 2016.

- [87] Richard P O’Neill, Paul M Sotkiewicz, Benjamin F Hobbs, Michael H Rothkopf, and William R Stewart Jr. Efficient market-clearing prices in markets with nonconvexities. *European journal of operational research*, 164(1):269–285, 2005.
- [88] Dimitris Bertsimas, Eugene Litvinov, Xu Andy Sun, Jinye Zhao, and Tongxin Zheng. Adaptive robust optimization for the security constrained unit commitment problem. *IEEE transactions on power systems*, 28(1):52–63, 2012.
- [89] David Pozo and Javier Contreras. Finding multiple nash equilibria in pool-based markets: A stochastic epec approach. *IEEE Transactions on Power Systems*, 26(3):1744–1752, 2011.
- [90] R Tyrrell Rockafellar, Stanislav Uryasev, et al. Optimization of conditional value-at-risk. *Journal of risk*, 2:21–42, 2000.
- [91] Philippe Artzner, Freddy Delbaen, Jean-Marc Eber, and David Heath. Coherent measures of risk. *Mathematical finance*, 9(3):203–228, 1999.